This is an *Accepted Manuscript*, which has been through the Royal Society of Chemistry peer review process and has been accepted for publication.

Accepted Manuscripts are published online shortly after acceptance, before technical editing, formatting and proof reading. Using this free service, authors can make their results available to the community, in citable form, before we publish the edited article. We will replace this *Accepted Manuscript* with the edited and formatted *Advance Article* as soon as it is available.

You can find more information about *Accepted Manuscripts* in the **Information for Authors**.

Enhancing Catalytic H_2 Evolution Performance of an Immobilised Cobalt Catalyst by Rational Ligand Design

Janina Willkomm, Nicoleta M. Muresan, Erwin Reisner[*]

Christian Doppler Laboratory for Sustainable SynGas Chemistry, Department of Chemistry, University of Cambridge, Lensfield Road, Cambridge CB2 1EW, UK

[*]*Corresponding author: email: reisner@ch.cam.ac.uk, web: http://www-reisner.ch.cam.ac.uk/*

1

Abstract

The catalyst [$Co^{III}Br((DO)(DOH)(4\text{-}BnPO_3H_2)(2\text{-}CH_2py)pn)]Br$, **CoP³**, has been synthesised to improve the stability and activity of cobalt catalysts immobilised on metal oxide surfaces. The **CoP³** catalyst contains an equatorial diimine-dioxime ligand, $(DOH)_2pn = N^2,N^{2'}$-propanediyl-bis(2,3-butanedione-2-imine-3-oxime), with a benzylphosphonic acid (4-$BnPO_3H_2$) group and a methylpyridine (2-CH_2py) ligand covalently linked to the bridgehead of the pseudo-macrocyclic diimine-dioxime ligand. The phosphonic acid functionality provides a robust anchoring group for immobilisation on metal oxides, whereas the pyridine is coordinated to the Co ion to enhance the catalytic activity of the catalyst. Electrochemical investigations in solution confirm that **CoP³** shows electrocatalytic activity for the reduction of aqueous protons between pH 3 and 7. The metal oxide anchor provides the catalyst with a high affinity for mesostructured Sn-doped In_2O_3 (*meso*ITO; loading of approximately 22 nmol cm^{-2}) and the electrostability of the attached **CoP³** was confirmed by cyclic voltammetry. Finally, immobilisation of the catalyst on ruthenium-sensitised TiO_2 nanoparticles in aqueous solutions in the presence of a hole scavenger establishes the activity of the catalyst in this photocatalytic scheme. The advantages of the elaborate catalyst design in **CoP³** in terms of stability and catalytic activity are shown by direct comparison with previously reported phosphonated Co catalysts. We therefore demonstrate that rational ligand design is a viable route for improving the performance of immobilised molecular catalysts.

Introduction

Solar fuels generation through artificial photosynthesis requires a well-balanced combination of light harvesting and charge separation with proton reduction and water oxidation catalysis, preferentially in a photoelectrochemical (PEC) cell.[1] As for H_2 evolution, molecular synthetic catalysts based on 3d transition metals like Fe^2, Co^3 or Ni^4 are currently under intensive investigation as an alternative to the current benchmark H_2 evolving catalysts: scarce and expensive Pt^5 and fragile enzymes known as hydrogenases.[6] However, the use of catalysts in a PEC cell requires their stable integration into electrodes, which is often challenging for molecular catalysts.[7]

An advantage of synthetic molecular catalysts compared to solid-state materials or enzymes is the relative ease to control and characterise their composition and to study their mechanisms and kinetics in great detail. This strength provides a rational route to elaborated and improved catalyst design through mechanistic understanding and often by adopting hydrogenase-related principles.[8] For example, bio-inspired nickel bis(diphosphine) catalysts were reported to generate H_2 photo-[9] and electrocatalytically[9-10] in aqueous solution. These Ni complexes remain electroactive when heterogenised on carbon-based electrodes,[11] and immobilisation on metal oxide nanoparticles[9] and on carbon nitride[12] has allowed for their exploitation for photocatalytic H_2 production in heterogeneous schemes. Synthetic mimics of the [FeFe]-hydrogenase active site evolve H_2 from water when combined with CdTe quantum dots as a photosensitiser[13] and when incorporated into a protective environment, *e.g.* a metal organic framework[14] or a micellar system.[15]

Cobalt catalysts with a bis(dimethylglyoximato) equatorial ligand (dmgH⁻) and an activity enhancing axial pyridine ligand,[3h,16] [CoCl(dmgH)$_2$(py)] (Figure 1A), have long been identified as one of the most active molecular catalysts for the reduction of aqueous protons and a wealth of experimental and theoretical information is available.[17] These catalysts

belong to the class of cobaloximes and they are also among the very few synthetic catalysts reported as O_2-tolerant during catalysis, which is an important consideration for their use in full water splitting systems.[16a,18] Cobaloximes have been integrated into photocatalytic systems by wiring the catalyst to a light absorber. For example, supramolecular homogeneous systems with a dye covalently linked to the Co catalyst,[19] colloidal systems containing dye-sensitised titania[20] or carbon nitride[21] and their immobilisation on photocathodes[22] have been reported. However, these assemblies suffer from the drawback of anchoring the cobaloxime to the light absorber *via* the monodentate axial pyridine ligand. The Co–pyridine bond becomes labile during catalysis, which results in the loss of the $Co(dmgH)_2$ core from the light absorber unit during irradiation.[19a,23] Consequently, the stability and performance of these photocatalytic systems are limited.
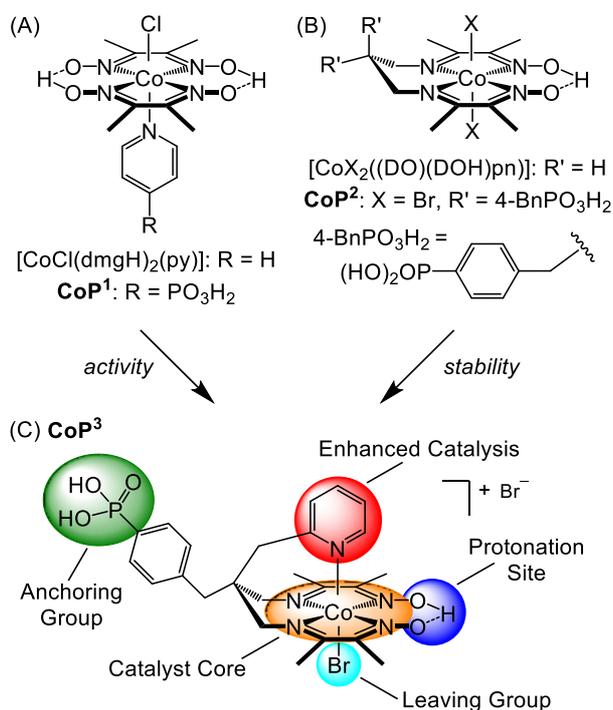

Figure 1. Chemical structures of (A) cobaloximes with an axial pyridine ligand, (B) cobalt diimine-dioxime catalysts, and (C) catalyst **CoP³** reported in this study. **CoP³** was designed to incorporate the activity enhancing pyridine of **CoP¹** (A),[20b] and the stable catalyst core and anchoring functionality of **CoP²** (B).[24]

A more robust class of cobalt catalysts, [CoX$_2$((DO)(DOH)pn)] with X = bromide or chloride and the tetradentate ligand (DOH)$_2$pn = N^2,$N^{2'}$-propanediyl-bis(2,3-butanedione-2-imine-3-oxime) (R' = H; Figure 1B),[3d,3i,25] was recently integrated into electrodes. This Co catalyst was immobilised on a carbon-based electrode *via* click chemistry (X = Cl, R' = H, N$_3$)[26] and on a conducting metal oxide electrode *via* a phosphonic acid linker (**CoP^2**, X = Br, R' = 4-BnPO(OH)$_2$; Figure 1B).[24,27] Anchoring of the Co catalyst through the propanediyl bridgehead of the pseudo-macrocyclic equatorial ligand provides a substantially more stable anchoring to an electrode than immobilisation *via* the axial pyridine in cobaloximes.

In this work, we present a cobalt catalyst for H$_2$ evolution, which does not only display good stability when anchored onto metal oxide surfaces, but also enhanced catalytic activity compared to the previously reported immobilised Co catalyst **CoP^2**. The novel cobalt catalyst, **CoP^3**, contains a pendant pyridine and a dangling phosphonic acid group linked to the bridgehead of the equatorial diimine-dioxime ligand (Figure 1C). The axial pyridine ligand coordinates to the metal centre and enhances the activity of the cobalt catalyst. Covalent linkage to the equatorial ligand framework ensures that the pyridine does not leave the catalyst core during turnover. The phosphonic acid group allows for attachment to metal oxide surfaces and is also tightly bound to the ligand framework. The electrochemistry of **CoP^3** in solution and when immobilised on mesoporous indium-tin oxide electrodes (ITO|*meso*ITO), as well as the photocatalytic activity of **CoP^3** in Ru-sensitised systems is reported and the results are directly compared with previously reported cobalt catalysts **CoP^1** and **CoP^2** (Figure 1).

Results and Discussion

Synthesis and Characterisation of CoP³

Complex **CoP³** was synthesised in six steps from commercially available starting materials with an overall yield of approximately 10% (Scheme 1 and ESI for experimental details).
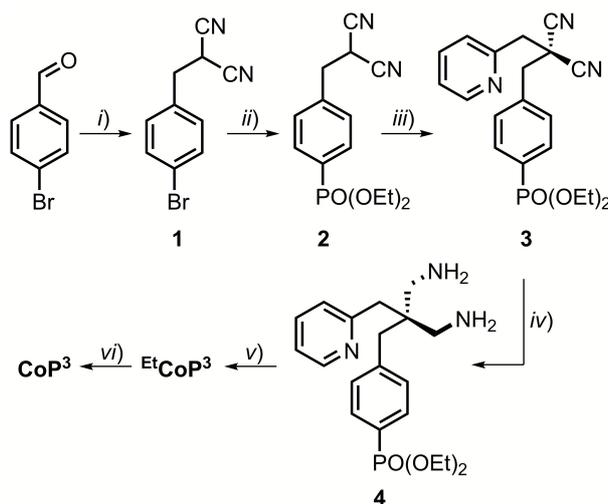
Scheme 1. *i*) Malononitrile, NaBH₄, ethanol/water (95/5), 3 h r.t., 80%; *ii*) HPO(OEt)₂, Et₃N, Pd(PPh₃)₄, PPh₃, tetrahydrofuran, 48 h, reflux, 73%; *iii*) 2-(bromomethyl)pyridine·HBr, K₂CO₃, acetone, 3d, r.t., 58%; *iv*) borane·tetrahydrofuran complex, tetrahydrofuran, 24 h, r.t., 99%; *v*) 2,3-butanedione monoxime, CoBr₂·6H₂O, methanol, 5d, r.t., 45%; *vi*) bromotrimethylsilane, dichloromethane, 48 h, r.t., 65%. The chemical structure of **CoP³** is shown in Figure 1C.

Compound **1** was prepared *via* condensation of 4-bromobenzaldehyde with malononitrile and reduction by NaBH₄.[28] The phosphonate ester derivative **2** was synthesised from **1** in a Pd-catalysed cross-coupling reaction with diethyl phosphite. Introduction of the pendant pyridine was achieved by alkylation of **2** with 2-(bromomethyl)pyridine. The resulting malononitrile derivative **3** was reduced to the diamine **4** by treatment with borane·tetrahydrofuran. Complex **ᴱᵗCoP³** was obtained from a three-step condensation-complexation-oxidation reaction:[24,25c] the desired diimine-dioxime ligand was prepared *via* condensation of **4** and 2,3-butanedione monoxime, followed by addition of CoBr₂·6H₂O to the crude ligand containing solution and oxidation of the Coᴵᴵ ion in air to form **ᴱᵗCoP³**. Hydrolysis of the phosphonate

ester using bromotrimethylsilane yielded the target complex **CoP³**. ¹H, ¹³C and ³¹P NMR spectra of the compounds are shown in Figures S1 to S11.

The final complex **CoP³** was characterised by ¹H, ¹³C, ³¹P and NOE NMR spectroscopy, UV-vis and ATR-IR spectroscopy, mass spectrometry and elemental analysis. The ³¹P NMR spectra of the phosphonate ester compounds **2-4** and **EtCoP³** feature a signal at approximately 19 ppm, which is shifted to 13 ppm in **CoP³** as expected upon hydrolysis of the phosphonate ester. Both cobalt complexes, **EtCoP³** and **CoP³** display a characteristic ¹H NMR signal at approximately 19 ppm, which is assigned to the O–H--O bridge proton of the equatorial (DO)(DOH)pn ligand.[24,29] ¹H NMR signals of the methylene protons on the propanediyl bridgehead of diamine **4** exhibit a downfield shift from 2.5 ppm to 3.7 and 4.1 ppm upon formation of the cobalt diimine-dioxime complex **EtCoP³**. Moreover, these diastereotopic methylene protons (^2J(H,H) = 15 Hz) show a significantly different chemical shift (for **CoP³**: $\Delta\delta$ = 0.6 ppm in DMSO-d_6). This difference is presumably due to two different axial ligands in the octahedral coordination sphere and is an indication of coordination of the pendant pyridine ligand to the metal centre in **EtCoP³** and **CoP³**. Evidence for coordination is also given by a 0.7 ppm upfield shift of the signal of the pyridine proton in 6-position upon formation of the cobalt complexes (H6, Table S1).[29] In addition, a NOE response was observed for this proton after saturation of the oxime proton signal at 19.2 ppm (Figure S12) revealing that both protons have to be in close proximity to each other.[29] When trifluoroacetic acid (TFA) was added to a solution of **CoP³** in DMSO-d_6, no shift of the pyridine proton signals was observed (Figure S13). If protonated, an additional set of signals would be expected in the range of 8 to 9 ppm.[30] Thus, the pyridine remains ligated to the cobalt centre and is not protonated even in the presence of a strong acid.

The ¹H NMR spectrum of **CoP³** in D_2O shows a similar upfield shift for the pyridine proton in 6-position as in DMSO-d_6 (7.8 ppm in **CoP³** *vs.* 8.5 ppm in diamine **4**) and the

7

spectrum remained unchanged for at least three weeks (Figure S14). Electronic absorption spectra of **CoP³** in water show a strong π-π^* absorption at λ = 259 and 219 nm (ε = $1.864 \cdot 10^4$ L mol^{-1} cm^{-1} and $2.774 \cdot 10^4$ L mol^{-1} cm^{-1}; Figure S15). Similar absorption features are obtained in pH 7 phosphate buffer and pH 4.5 acetate buffer and no changes in the UV-vis spectrum were apparent when the solution was acidified with TFA (Figure S15), demonstrating the good stability of the catalyst in aqueous solutions.

Electrochemical Studies in Solution

The electrochemical response of **CoP³** was investigated in organic as well as aqueous electrolyte solutions using a three-electrode set-up with a glassy carbon working electrode (0.07 cm^2). A cyclic voltammogram (CV) of **CoP³** recorded in DMF/TBABF$_4$ electrolyte solution (TBABF$_4$ = tetrabutylammonium tetrafluroborate, 0.1 M) exhibits two reversible one-electron reduction waves at $E_{1/2}$ = –0.67 V and –1.07 V *vs.* Fc$^+$/Fc, which are assigned to the Co^{III}/Co^{II} and Co^{II}/Co^{I} redox couples, respectively (Figure S16A).[3i,24] Upon addition of 1 to 10 equivalents of TFA, a catalytic proton reduction wave appeared close to the potential of the initial Co^{II}/Co^{I} redox couple at a half-wave potential, $E_{1/2}$, of –1.06 V *vs.* Fc$^+$/Fc, (Figure S16B). Thus, an overpotential (η) of approximately 110 mV is required to reduce TFA protons (E^0(H$^+$/H$_2$) = –0.95 V *vs.* Fc$^+$/Fc for 10 mM TFA in DMF)[31] with **CoP³**, which is comparable to previously reported [Co(DO)(DOH)pn]-type complexes.[3i,24]

CVs recorded in aqueous Britton-Robinson buffer (pH 3 to 7) feature a reversible Co^{III}/Co^{II} redox couple and quasi-reversible Co^{II}/Co^{I} reduction (Figure 2A). When scanning towards more cathodic potential, a third reduction wave is observed which is attributed to catalytic proton reduction by the complex (Figure 2A).[3d] Comparable electrochemical responses were obtained when a pH 7 triethanolamine (TEOA)/Na$_2$SO$_4$ electrolyte solution and pH 4.5 acetate or ascorbic acid (AA) solution were used (Figure S17), except that no

Co^{III}/Co^{II} reduction wave can be observed in cathodic scans in AA solution, presumably due to the chemical reduction of **Co^{III}P^3** to **Co^{II}P^3** (Figure S18). The onset of a weak wave, tentatively assigned to Co^{II}/Co^{III} oxidation, is observed at approximately 0.05 V *vs.* NHE before AA oxidation starts at 0.2 V *vs.* NHE.

The pH-dependent investigation also revealed that the half-wave potential of the catalytic reduction wave, $E_{cat/2}$, shifts by approximately −60 mV per pH unit increase (Figure 2A); in agreement with a one proton–one electron coupled process according to the Nernst equation. This was previously attributed to protonation of the oxime functionality in [Co(DO)(DOH)pn]-type complexes.[3i,25a]
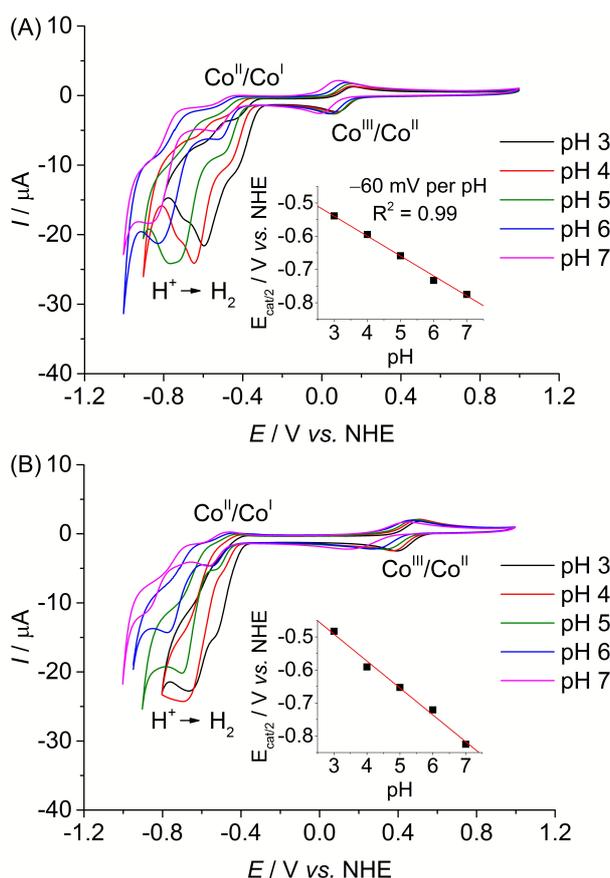

Figure 2. CVs of (A) **CoP^3** and (B) **CoP^2** (0.8 mM) recorded in an aqueous Britton-Robinson buffer at different pH values on a glassy carbon working electrode at 20 mV s$^{−1}$. The insets show the correlation between the half-wave potential of the catalytic reduction wave, $E_{cat/2}$, and the pH value. The red traces represent the linear fit of the data points.

9

Comparison of the electrochemical response of **CoP³** to the previously reported complex **CoP²** allows us to elucidate any beneficial effect of the additional axial pyridine ligand on the proton reduction activity. CVs of **CoP²** recorded in the pH range from 3 to 7 are shown in Figure 2B. For both cobalt diimine-dioxime catalysts, the catalytic reduction wave decreases with increasing pH indicating a higher proton reduction activity under more acidic conditions, which has been previously observed for (DO)(DOH)pn-type cobalt catalysts.[26] Peak currents of the catalytic reduction wave, I_{cat}, and I_{cat}/I_p ratios taking into account the non-catalytic Co^{III}/Co^{II} reduction peak currents, I_p, are similar for both complexes at pH 3 and 4 (Table S2). But, **CoP³** features higher I_{cat} and I_{cat}/I_p ratios at pH values above 4 revealing a higher activity of **CoP³** under more pH neutral conditions (Table S2). Moreover, the half wave potential $E_{cat/2}$ of **CoP³** is observed at less negative potentials than for **CoP²** under pH neutral conditions ($-$ 0.83 V for **CoP²** *vs.* $-$ 0.78 V for **CoP³**).

The half-wave potential, $E_{1/2}$, of the Co^{II}/Co^{I} reduction wave in **CoP³** shifts with about -33 mV per pH at pH values below 6 and becomes almost pH independent above pH 6 (Figure S19A). Such a change in slope was not observed for $E_{1/2}(Co^{II}/Co^{I})$ in **CoP²** (Figure S19B), suggesting an alteration in the coordination sphere specific to **CoP³**, *e.g.* a ligated and non-ligated, probably protonated pendant pyridine ligand. The pH-dependencies of $E_{1/2}$ of the Co^{III}/Co^{II} reduction wave change in a similar manner for **CoP²** and **CoP³** (Figure S20) and are ascribed to protonation/deprotonation occurring at moieties present in both complexes, *e.g.* at phosphonic acid groups[9] or aquo ligands. Due to a different number of those functionalities the slopes differ for both complexes.

Based on these findings, we suggest that the enhanced catalytic activity of **CoP³** under near neutral conditions is due to coordination of the pyridine to the cobalt centre during the catalytic cycle. The electron donating ability of the pyridine ligand would allow for the formation of a more basic Co-hydride species in the rate limiting step of the catalytic cycle,

thereby improving proton reduction catalysis.[16a,32] A similar increase of catalytic current and decrease in overpotential has previously been observed when an axial pyridine ligand was introduced to the coordination sphere of cobaloxime complexes at neutral pH.[16a] Addition of one and four equivalents of pyridine to a **CoP²**-containing electrolyte solution pH 7 lead to the formation of a species probably similar to **CoP³** as evident from the appearance of a fully reversible Co^{III}/Co^{II} couple (Figure S21). However, it did not result in any increase of the catalytic reduction wave which demonstrates that the covalent integration of the pyridine as achieved in **CoP³** is also critical to enhance the activity of the cobalt diimine-dioxime catalyst.[25c]

The comparable pH-dependent shifts of $E_{1/2}(Co^{II}/Co^{I})$ for **CoP²** and **CoP³** below pH 6 suggest a temporary non-coordinated pyridine in **CoP³** upon reduction. Although the axial pyridine in **CoP³** is coordinated to the cobalt centre in the initial Co^{III} state even in the presence of a strong acid (see above), reduction to Co^{II} or a formal Co^{I} species results in a labile Co–pyridine bond and subsequent release of the pyridine from the Co ion. However, the covalently linked pyridine ligand remains in close proximity to the cobalt centre and could improve catalysis in two distinct ways. It could be partially protonated under acidic conditions (pK_a of 2-picoline: 5.96)[33] and consequently act as a proton relay in the catalytic cycle or it could readily re-coordinate and enhance activity as described above. The fully reversible Co^{III}/Co^{II} redox couple indicates that the pyridine re-coordinates to the Co centre upon oxidation of the complex.

Finally, both Co diimine-dioxime catalysts were compared to the phosphonated cobaloxime catalyst **CoP¹**. Among the series of phosphonated cobalt catalyst, **CoP¹** is the most active proton reduction catalyst at neutral pH, featuring a large proton reduction wave at more positive potential than **CoP²** and **CoP³** (Figure S17A). Under more acidic conditions, no Co^{II} to Co^{III} oxidation wave was observed for **CoP¹** in the anodic reverse scans (Figure

11

S17B and S18A) indicating catalyst decomposition due to hydrolysis of the equatorial $(dmgH^-)_2$ ligand.[34]

Electrochemical Studies with Heterogenised Catalysts

The phosphonic acid anchoring groups in CoP^n (n = 1 to 3) allow for the grafting of the complexes onto metal oxide surfaces.[20,24] The electrochemical response of the three cobalt catalysts immobilised onto mesoporous Sn-doped In_2O_3 on (ITO|*meso*ITO) electrodes was compared to determine the loading of the Co catalysts to a metal oxide surface and the stability during voltammetry, specifically when cycling between the Co^{III}, Co^{II} and Co^I oxidation states. The electrodes were prepared from ITO nanoparticles as described previously[24] and were loaded with catalysts by immersing a cleaned slide into a 6 mM catalyst solution in dry DMF for 15 h. The ITO|*meso*ITO|CoP^n electrodes were gently rinsed with fresh DMF, dried under N_2 and studied in a CoP^n-free DMF/TBABF$_4$ electrolyte (0.1 M).

CVs of the ITO|*meso*ITO|CoP^3 electrode in DMF/TBABF$_4$ electrolyte are shown in Figure 3. A linear correlation between the peak current density, J_P, of the reversible Co^{II}/Co^I reduction at $E_{1/2} = -1.03$ V *vs.* Fc$^+$/Fc and the scan rate, v, confirms that CoP^3 is immobilised on the ITO|*meso*ITO surface. The disappearance of the Co^{III}/Co^{II} redox couple for the immobilised complex at $E_{1/2} = -0.69$ V *vs.* Fc$^+$/Fc with the concomitant appearance of a new wave at $E_{1/2} = -0.43$ V *vs.* Fc$^+$/Fc during consecutive scans is presumably due to a gradual replacement of the axial bromido ligand by DMF. Upon reduction, the bromido ligand dissociates from the Co centre, leaving a five-coordinated Co^{II} and Co^I species with a free coordination site.[16b] When re-oxidised to Co^{III}, the free site is occupied by the solvent DMF, which results in an anodic shift of the redox potential.[35] CVs of ITO|*meso*ITO|CoP^2 show comparable features in DMF/TBABF$_4$ electrolyte solution (Figure S22 and S23B). The

determination of any J_P-v correlation was not possible for ITO|*meso*ITO|**CoP^1** due to the poor

stability of the immobilised **CoP^1** on ITO and subsequent rapid decrease of the redox waves
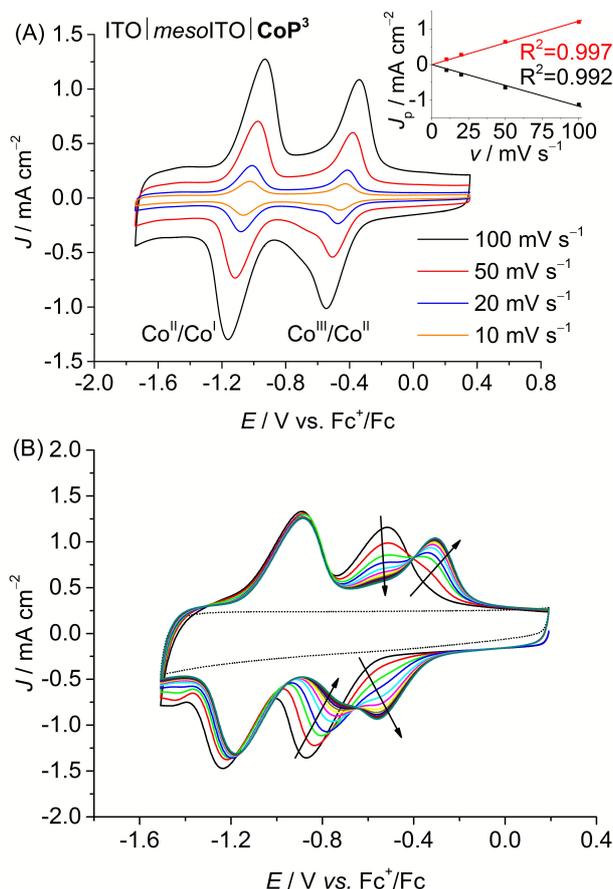
within the first few scans (Figure S23A; see below).

Figure 3. (A) CVs of ITO|*meso*ITO|**CoP^3** in DMF/TBABF$_4$ electrolyte (0.1 M) at different scan rates (10, 20, 50, 100 mV s^{-1}). Inset: The correlation between the peak current density, Jp (Co^{II}/Co^{I}), and scan rate, v, is shown. The black and red traces represent linear fits to the data points. (B) Consecutive CVs of ITO|*meso*ITO|**CoP^3** in DMF/TBABF$_4$ electrolyte (0.1 M) at a scan rate of 100 mV s^{-1}. The background of ITO|*meso*ITO without catalyst is shown as dotted line.

The amounts of catalyst immobilised onto the mesoporous ITO electrodes were

estimated by integration of the redox waves (reduction and oxidation) from the first CV scans

in DMF/TBABF$_4$ electrolyte solution (Table 1). Loadings between 22 and 28 nmol cm^{-2}

(referenced to the geometrical surface area of the electrode) were determined for the three

ITO|*meso*ITO|**CoP^n** electrodes. We only observed small differences in the loadings, which

might be due to different spatial demands of the catalysts. Comparable results and trends were obtained when the integration of the redox waves was performed with CV scans recorded in aqueous electrolyte solution (Table S3, Figures S24 and S25) and loadings are comparable to a previously reported Ru-based compound on mesostructured ITO.[36] The results show that **CoP³** binds well and with a comparable loading to **CoP²** to the metal oxide electrode despite only having one anchoring group.

Table 1. Loading of the three **CoPⁿ** catalysts per geometrical surface area of ITO|*meso*ITO|**CoPⁿ** electrodes as determined by integrating redox waves in CV traces recorded in DMF/TBABF₄ electrolyte.

Catalyst	n (CoPⁿ) / nmol cm^{-2}	
	first scan[a]	10th scan[b]
CoP¹	25.6 ± 1.1	5.6 ± 0.5
CoP²	28.1 ± 2.8	28.5 ± 3.6
CoP³	22.5 ± 1.5	22.7 ± 0.7

[a]Mean value with standard deviation (σ) for the first CV scan; [b]Mean value with standard deviation (σ) for CVs after 10 scans at 100 mV s^{-1}.

After 10 consecutive scans practically no desorption of **CoP³** and **CoP²** was observed, whereas approximately 80% of **CoP¹** was lost from the ITO|*meso*ITO electrode (Table 1). As discussed above, reduction of low spin Co^{III} results in a labile Co^{II} and Co^{I} species, which leads to the loss of the Co(dmgH)₂ core from the ITO-anchored phosphonated pyridine in **CoP¹**.[7b] This instability was not observed for **CoP²** and **CoP³**, demonstrating the much improved robustness when anchoring the cobalt catalysts with one (**CoP³**) or two (**CoP²**) phosphonic acid groups on the tetradendate equatorial (DO)(DOH)pn-ligand to the ITO electrode (Figure 3 and S23B).[24] **CoP³** therefore displays much higher stability on an electrode than **CoP¹** and is significantly more active as a proton reduction catalyst than **CoP²** as shown by electrochemical investigation in solution.

14

Photocatalytic Studies

The photocatalytic activity of the **CoP^n** catalysts was studied in solution and in heterogeneous suspension systems containing either TiO_2 or ZrO_2 nanoparticles with TEOA (0.1 M, pH 7) or AA (0.1 M, pH 4.5) as buffer and sacrificial electron donor (SED). $[Ru^{II}(2,2'$-bipyridine$)_2(2,2'$-bipyridine-4,4'-bisphosphonic acid$)]Br_2$ (**RuP**, Figure 4A) was used as photosensitiser. Photoexcited **RuP** (**RuP***) can operate through an oxidative $(E^0(\mathbf{RuP^+}/\mathbf{RuP^*})$ = –0.95 V *vs.* NHE)[37] or reductive quenching mechanism $(E^0(\mathbf{RuP^*}/\mathbf{RuP^-})$ = 1.07 V *vs.* NHE),[38] which would generate **RuP$^-$** $(E^0(\mathbf{RuP}/\mathbf{RuP^-})$ = –1.05 V *vs.* NHE).[9,38-39] Photoinduced electron transfer from the generated **RuP** species to the **CoP^n** catalyst can occur either directly (homogeneous system; Figure 4B) or *via* the injection of electrons into the conduction band (CB) of the semiconductor TiO_2 (E_{CB} = –0.70 V *vs.* NHE at pH 7; E_{CB} = –0.55 V *vs.* NHE at pH 4.5)[40] by a '*through particle*' mechanism (Figure 4C).[9] **RuP*** and **RuP$^-$** are unable to transfer electrons into the more negative CB of ZrO_2 (E_{CB} = –1.26 V *vs.* NHE at pH 4.5, E_{CB} = –1.40 V *vs.* NHE at pH 7),[41] which only allows for direct electron transfer from photoexcited **RuP** to the catalyst as in the homogeneous system (Figure 4C). A comparison of the electrocatalytic onset potentials for proton reduction of the **CoP^n** catalysts with the thermodynamic driving force from **RuP** and the semiconductors is summarised in Figure 4D. It illustrates that photo-H_2 evolution is thermodynamically possible with all three catalysts, but kinetic factors may have a detrimental effect on some of the systems.[42]

In a standard experiment, 0.1 μmol **CoP^n** and 0.1 μmol **RuP** were used in 2.25 mL of aqueous solution containing the SED (homogeneous **RuP|CoP^n** system) and 5 mg of metal oxide nanoparticles were added for the particle systems (**RuP|TiO$_2$|CoP^n** or **RuP|ZrO$_2$|CoP^n**). The samples were kept at 25 ºC and irradiated with visible light from a solar light simulator equipped with an AM 1.5G, IR and UV filter (λ > 420 nm). The activity

15

is expressed as Co-based turnover number, TON_{Co} (mol H_2 per mol CoP^n), which was

obtained after four hours of visible light irradiation (Table 2). At this point, all systems had

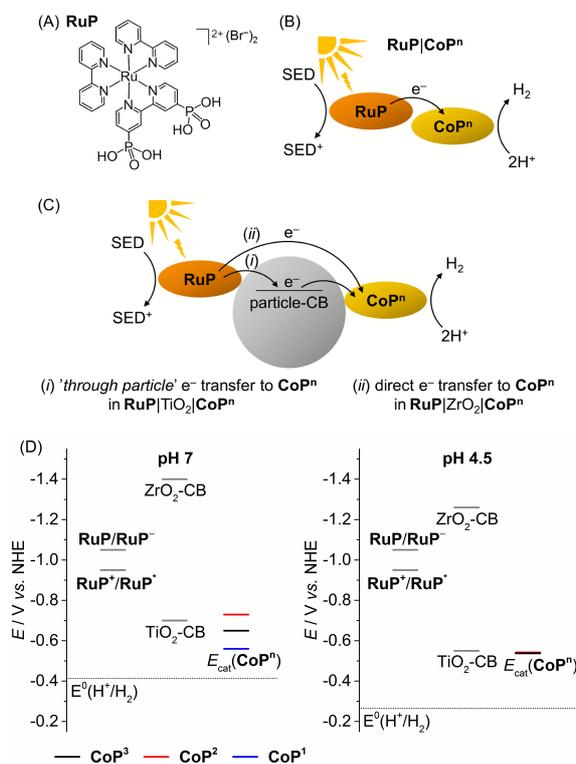lost their photoactivity under these standard conditions.

Figure 4. (A) Chemical structure of the photosensitiser **RuP**. (B and C) Electron transfer mechanisms from the photoexcited **RuP** dye to the catalyst CoP^n in the homogenous and heterogeneous suspension systems with TiO_2 and ZrO_2 particles. The '*through particle*' electron transfer pathway is only accessible in **RuP**|TiO_2|CoP^n (see text). (D) Schematic energy diagram with the redox potentials of RuP^* and RuP^- generated upon photoexcitation, conduction band potentials of the semiconductor particles (TiO_2-CB and ZrO_2-CB), the thermodynamic redox potential for proton reduction, $E^0(H^+/H_2)$, and the catalytic proton reduction onset potentials, E_{cat}, of the CoP^n catalysts determined from CVs in $TEOA/Na_2SO_4$ (0.1 M each, pH 7) and acetate electrolyte (0.1 M, pH 4.5).

We first investigated the photocatalytic activity of CoP^3 in pH 7 TEOA solution. No

H_2 was generated in the **RuP**|CoP^3 and **RuP**|ZrO_2|CoP^3 systems. **RuP**|TiO_2|CoP^3 produced a

TON_{Co} of 12.3 ± 0.3 during 4 h visible light irradiation (Figure 5A). No H_2 or only trace

amounts of H_2 were detectable when omitting CoP^3, **RuP**, SED or light from this system or

when CoBr$_2$ was added instead of **CoP^3** (Table S5). Increasing the concentration of **CoP^3** in **RuP**|TiO$_2$|**CoP^3** to 0.2 μmol resulted in a slight enhancement in the overall TON$_{Co}$ (16.5 ± 0.5; Figure 26A). The highest TON$_{Co}$ of 22.0 ± 1.5 was observed when the amount of **RuP** was increased to 0.2 μmol (Table S4, Figure S26B).
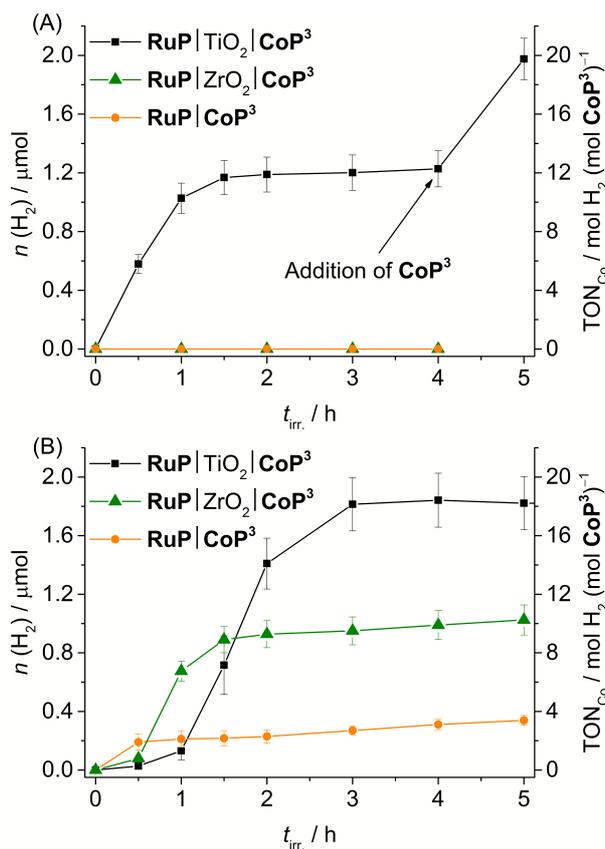

Figure 5. Photoactivity of **CoP^3** expressed as total amount of headspace H$_2$ over irradiation time and TON$_{Co}$ (AM 1.5G, 100 mW cm^{-2}, λ > 420 nm) in different systems (**RuP**|TiO$_2$|**CoP^3**, **RuP**|ZrO$_2$|**CoP^3** and **RuP**|**CoP^3**) in (A) pH 7 TEOA buffer (2.25 mL, 0.1 M) and (B) pH 4.5 AA buffer (2.25 mL, 0.1 M). A 1:1 ratio of **CoP^3** and **RuP** (0.1 μmol each) was used and either 5 mg of TiO$_2$ or ZrO$_2$ were added in case of particle systems.

Table 2. Results of visible light driven H_2 evolution with **CoP^n** and **RuP** in solution or in particle suspensions with TiO_2 or ZrO_2.[a]

	TOF_{Co} (1 h)[b] / h^{-1}	TON_{Co} (4 h)[c]	n (H_2) / μmol (4 h)[c]
pH 7 (TEOA):			
RuP|CoP^3	–	–	< 0.03[d]
RuP|ZrO$_2$|CoP^3	–	–	< 0.03[d]
RuP|TiO$_2$|CoP^3	10.3 ± 0.4	12.3 ± 0.3	1.23 ± 0.03
RuP|TiO$_2$|CoP^3$_{centr.}$[e]	*n.d.*[f]	*n.d.*[f]	0.74 ± 0.27
RuP|TiO$_2$|CoP^2	0.6 ± 0.02	2.4 ± 0.1	0.24 ± 0.01
RuP|TiO$_2$|CoP^1	44.0 ± 0.9	56.6 ± 2.2	5.66 ± 0.22
RuP|TiO$_2$	*n.d.*[f]	*n.d.*[f]	0.14 ± 0.07
pH 4.5 (AA):			
RuP|CoP^3	2.1 ± 0.6	3.1 ± 0.4	0.31 ± 0.04
RuP|ZrO$_2$|CoP^3	8.1 ± 2.2[g]	9.9 ± 0.2	0.99 ±0.02
RuP|TiO$_2$|CoP^3	12.8 ± 0.6[g]	18.4 ± 0.5	1.84 ± 0.05
RuP|TiO$_2$|CoP^2	1.2 ± 0.2	1.2 ± 0.08	0.12 ± 0.01
RuP|TiO$_2$|CoP^1	–	–	< 0.03[d]
RuP|TiO$_2$, no CoP^3	–	–	< 0.03[d]
RuP|ZrO$_2$, no CoP^3	*n.d.*[f]	*n.d.*[f]	0.09 ± 0.02
RuP, no CoP^3	–	–	< 0.03[d]

[a]The following standard conditions were employed unless otherwise noted: AM 1.5G, 100 mW cm^{-2}, λ > 420 nm irradiation, 0.1 μmol of **CoP^n** and 0.1 μmol of **RuP** in homogenous solution or in suspensions with TiO_2 or ZrO_2 nanoparticles (5 mg) in aqueous TEOA or AA solution (2.25 mL, 0.1 M). Mean values ± standard deviation (σ) given from at least three different reaction vessels. [b]TOF based on **CoP^n** for the first hour of irradiation. [c]TON based on **CoP^n** and total of headspace H_2 accumulated after four hours irradiation. [d]Below the limit of detection by gas chromatography. [e]Particles were loaded with the catalyst and the dye, centrifuged and re-suspended in fresh buffer solution prior to use. [f]*n.d.* = not defined (no **CoP^3** present or amount of **CoP^3** not precisely known). [g]TOF is based on the maximum H_2 evolution rate after the initial lag period.

The lack of photo-H_2 evolution in the homogeneous and ZrO_2-containing systems suggests that **RuP**[*] is not capable of reducing **CoP³** directly to initiate proton reduction which is in agreement with the previously reported inactivity of **RuP|ZrO₂|CoP¹**, **RuP|CoP¹** and a [CoBr₂((DO)(DOH)pn)] complex in combination with a Ru-dye and triethylamine as SED in solution.[20a,25b,39] A possible explanation may be that the more reducing **RuP⁻** is not generated in aqueous TEOA solution.[43] Addition of TiO_2 facilitates oxidative quenching of **RuP**[*] and charge separation which allows for efficient electron transfer from **RuP** to **CoP³** *via* its CB in a '*through particle*' mechanism, thereby triggering photoactivity of this system.[20a,39] A comparable, surface-linker free cobalt diimine-dioxime catalyst with a pendant pyridine ligand was studied in solution using a Re photosensitiser and TEOA as sacrificial agent. A Co-based TON_{Co} of approximately 15 has been reported for this homogeneous photocatalytic system under near neutral conditions (pH 7.7).[25c] The cobalt diimine-dioxime catalyst with a pendant pyridine ligand therefore keeps the full activity when immobilised on a semiconductor as is evident from the maximum TON_{Co} of 22.0 ± 1.5 observed with **RuP|TiO₂|CoP³**.

Photo-H_2 evolution activity of the deactivated **RuP|TiO₂|CoP³** system was fully recovered by addition of fresh **CoP³** to the suspension (Figure 5A) indicating complete degradation of **CoP³** within the first few hours of photocatalysis. To date, no detailed studies on possible degradation products of Co(DO)(DOH)pn catalysts are available, but partial regeneration of the catalyst by addition of fresh (DOH)₂pn ligand to a deactivated system was reported, which suggests ligand degradation, most likely through hydrogenation.[25b,44] The reduction of **CoP³** could also lead to a ligand radical species ($Co^{II}L^{\cdot}$, L = ligand) instead of the formal Co^I species.[24] Reductive coupling of two $Co^{II}L^{\cdot}$ radical species might result in the formation of catalytically inactive dimer complexes.[45] The formation of a Co-containing solid-state deposit would be another possible degradation pathway.[46] However,

photocatalysis completely ceased after several hours of visible light irradiation and the activity could be only recovered by addition of fresh catalyst. This result supports a molecular active species in the **RuP**|TiO$_2$|**CoP^3** system.

When stirring **CoP^3** (0.1 μmol) with 5 mg TiO$_2$ in an aqueous pH 7 TEOA solution, approximately 60% of the catalyst was attached to the particles as determined by spectrophotometry following $\lambda = 259$ nm (Figure S27A). **RuP** binds well to TiO$_2$ and approximately 80% ($\lambda_{max} = 288$ and 457 nm) were adsorbed in the presence of 0.1 μmol **CoP^3** (Figure S27B). The overlap of the strong absorption bands in **RuP** prevented the accurate determination of the **CoP^3** loading in the presence of **RuP**. Approximately 60% of photocatalytic activity remained (0.74 ± 0.27 μmol H$_2$) when the excess of **CoP^3** and **RuP** were removed from the pre-loaded particles by centrifugation and re-suspension of **RuP**|TiO$_2$|**CoP^3** in a fresh buffer solution (Table 2). This observation agrees well with the observed loading for **CoP^3** and shows that the majority of attached **CoP^3** remained on the particle surface and was not replaced by the dye (5 mg P25 TiO$_2$ nanoparticles have a loading capacity of approximately 0.25 μmol **RuP**).[6d]

Full spectrum irradiation (AM 1.5G, 100 mW cm^{-2}, no filter) of dye-free TiO$_2$|**CoP^3** resulted in a TON$_{Co}$ of 17.2 ± 1.3. The photo-H$_2$ production activity decreased by 97% when phosphate buffer (50 mM, pH 7) was added to the system (Figure S28). The phosphate anions and the phosphonic acid group in **CoP^3** compete for surface binding sites on TiO$_2$. This experiment demonstrates that binding of **CoP^3** to the TiO$_2$ nanoparticle *via* the ($-$PO$_3$H$_2$) anchoring group is essential for effective electron transfer from the TiO$_2$ conduction band to the catalyst[20a] and further supports that a molecular catalyst rather than a solid state deposit is active on TiO$_2$.

Finally, an unoptimised external quantum efficiency (EQE) of 0.35 ± 0.02 % was determined for the **RuP**|TiO$_2$|**CoP^3** system (0.1 μmol **RuP**, 5 mg TiO$_2$, 0.2 μmol **CoP^3**) in an

aqueous pH 7 TEOA solution (0.1 M) after 1 h irradiation at λ = 465 nm (I = 22 mW cm^{-2}), which is close to the absorption maximum of **RuP** (λ_{max} = 455 nm). This value is comparable to the previously reported EQE for **RuP**|TiO$_2$|**CoP**^{1} (1.0 ± 0.2 %)[39] and colloidal systems containing carbon nitrides and molecular Ni catalysts (0.37 and 1.51 %).[12,47]

In pH 4.5 AA solution, a TON$_{Co}$ of 18.4 ± 0.5, 9.9 ± 0.2 and 3.1 ± 0.4 was observed with **RuP**|TiO$_2$|**CoP**^{3}, **RuP**|ZrO$_2$|**CoP**^{3} and **RuP**|**CoP**^{3}, respectively (Table 2, Figure 5B). The three systems were completely deactivated after 4 h of visible light irradiation. Control experiments with CoBr$_2$ instead of **CoP**^{3} and in the absence of **CoP**^{3}, **RuP**, electron donor or light showed no or only trace amounts of H$_2$ (Table S8). The different activity of the three systems can be explained by two different mechanisms occurring under these experimental conditions (pH 4.5, AA). Previous studies have shown that **RuP*** is readily quenched oxidatively on TiO$_2$ by electron transfer to the TiO$_2$ conduction band in the picosecond time-scale,[9,48] whereas **RuP*** undergoes reductive quenching by AA to generate **RuP**$^-$ in solution or in the ZrO$_2$ system.[9] Inefficient photocatalytic H$_2$ evolution has been previously reported for [CoX$_2$(DO)(DOH)pn] complexes in combination with a Ru-dye in AA.[49] The oxidative quenching pathway in the TiO$_2$-containing system provides a possible explanation for the improved photocatalytic activity of **RuP**|TiO$_2$|**CoP**^{3}.

The initial lag period of photo-H$_2$ evolution in AA was dependent on the ratio of **CoP**^{3} to **RuP** and is presumably due to the slow accumulation of Co^I species, which is required to enter the catalytic cycle. An increased lag phase with enhanced photostability and a higher final TON$_{Co}$ was observed in all three photocatalytic systems when changing the **CoP**^{3}:**RuP** ratio from 1:1 to 2:1. At a **CoP**^{3}:**RuP** ratio of 1:2, a reduced lag phase with a shorter lifetime of photocatalysis and a somewhat lower final TON$_{Co}$ is achieved (Table S7, Figure S29). Recovery of the photocatalytic activity of **RuP**|TiO$_2$|**CoP**^{3} by addition of either fresh **CoP**^{3} or **RuP** was not successful suggesting simultaneous degradation of both, dye and

catalyst. By providing new **CoP³** and **RuP**, the initial photocatalytic activity of the **RuP**|TiO₂|**CoP³** system could be regained (Figure S30). Photo-degradation of **RuP** in AA has been observed previously.[9] Similar pathways as discussed above might account for degradation of the catalyst in an aqueous AA solution.

Finally, the photocatalytic activity of the colloidal **RuP**|TiO₂|**CoP³** system was compared to the activity of **CoP¹** and **CoP²** using standard conditions (0.1 μmol **CoP^n** and 0.1 μmol **RuP** on 5 mg TiO₂). In TEOA buffer (0.1 M, pH 7), a TON_{Co} of 56.6 ± 2.2 was obtained for **CoP¹**,[20b] whereas the **RuP**|TiO₂|**CoP²** system only produced small amounts of H₂ (TON_{Co} = 2.4 ± 0.1; Table 2, Figure S31A). In AA at pH 4.5, only traces of H₂ were produced with **CoP¹**, which is catalytically unstable under acidic conditions (see above). A TON_{Co} of approximately 1 was achieved for **CoP²** during 4 h visible light irradiation in AA (Table 2, Figure S31B).

The results from photocatalytic experiments are in agreement with trends observed during electrochemical investigation of the three catalysts: **CoP¹** shows the fastest turnover rate at neutral pH, whereas **CoP³** is the most active catalyst in an aqueous acidic solution. However, **CoP³** is the best and most suitable catalyst when activity *and* stability on the metal oxide surface are taken into account. **CoP²** displays strong attachment to metal oxides, but it shows overall modest catalytic activity. **CoP¹** is not stable during turnover in a pH 4.5 AA solution and can therefore not act as a catalyst under acidic conditions. The high photoactivity of **CoP¹** at pH 7 despite its labile anchoring to **RuP**|TiO₂ particles in the colloidal suspension can be explained as follows: the Co(dmgH)₂ core of **CoP¹** is released during catalysis but can re-coordinate to a TiO₂-anchored pyridine ligand ('hop-on hop-off mechanism') through a high probability of collision in the bulk of the suspension. When **CoP¹** is immobilised on an electrode such as ITO|*meso*ITO, however, the Co(dmgH)₂ core

will be released from the surface and will diffuse into the bulk solution, where it will not readily diffuse back to the electrode surface.

Conclusions

In summary, a new cobalt diimine-dioxime H_2 evolution catalyst (**CoP³**) is described that features a stable binding site for attachment to metal oxide surfaces *and* a pendant pyridine ligand to enhance the catalytic activity. **CoP³** was prepared in six steps and characterised by NMR, UV-vis and ATR-IR spectroscopy, mass spectrometry and elemental analysis. Electrochemical investigation of the new catalyst revealed that it is electrocatalytically active for proton reduction in aqueous solution over a wide pH range. **CoP³** attaches with high loading and good stability to a mesostructured Sn-doped In_2O_3 electrode. We demonstrate that **CoP³** produces H_2 photocatalytically in dye-sensitised systems under visible light irradiation at neutral and acidic pH with different sacrificial reagents and showed that H_2 evolution is improved in the presence of TiO_2 particles compared to homogeneous systems. **CoP³** displays significant advantages over previously reported immobilised Co catalysts as it shows a higher catalytic proton reduction activity *and* provides a strong and more stable anchoring to metal oxides surfaces on electrodes.

Overall, our work emphasises the necessity for elaborated molecular catalyst design with regard to the assembly of efficient (photo-)electrodes with molecular catalysts and their application in (photo-)electrochemical cells. The availability of thorough experimental and theoretical studies for cobaloxime and cobalt diimine-dioxime catalysts enabled us to rationally design a catalyst with improved activity *and* stability on electrodes. It also provides a solid basis for further optimisation of this class of cobalt catalysts and their successful integration into PEC devices in the future.

Associated Content

Author Information

Corresponding Author: *reisner@ch.cam.ac.uk*

Acknowledgements

References

1 (a) P. Bornoz, F. F. Abdi, S. D. Tilley, B. Dam, R. van de Krol, M. Graetzel and K. Sivula, *J. Phys. Chem. C*, 2014, **118**, 16959-16966; (b) J. Yang, D. Wang, H. Han and C. Li, *Acc. Chem. Res.*, 2013, **46**, 1900-1909; (c) J. Barber and P. D. Tran, *J. R. Soc. Interface*, 2013, **10**, 20120984; (d) C.-Y. Lin, Y.-H. Lai, D. Mersch and E. Reisner, *Chem. Sci.*, 2012, **3**, 3482-3487.

2 (a) G. P. Connor, K. J. Mayer, C. S. Tribble and W. R. McNamara, *Inorg. Chem.*, 2014, **53**, 5408-5410; (b) M. J. Rose, H. B. Gray and J. R. Winkler, *J. Am. Chem. Soc.*, 2012, **134**, 8310-8313; (c) S. Kaur-Ghumaan, L. Schwartz, R. Lomoth, M. Stein and S. Ott, *Angew. Chem. Int. Ed.*, 2010, **49**, 8033-8036; (d) A. M. Kluwer, R. Kapre, F. Hartl, M. Lutz, A. L. Spek, A. M. Brouwer, P. W. N. M. van Leeuwen and J. N. H. Reek, *Proc. Natl. Acad. Sci.*, 2009, **106**, 10460-10465; (e) G. A. N. Felton, A. K. Vannucci, J. Chen, L. T. Lockett, N. Okumura, B. J. Petro, U. I. Zakai, D. H. Evans, R. S. Glass and D. L. Lichtenberger, *J. Am. Chem. Soc.*, 2007, **129**, 12521-12530; (f) C. Tard, X. Liu, S. K. Ibrahim, M. Bruschi, L. D. Gioia, S. C. Davies, X. Yang, L.-S. Wang, G. Sawers and C. J. Pickett, *Nature*, 2005, **433**, 610-613.

3 (a) L. Chen, M. Wang, K. Han, P. Zhang, F. Gloaguen and L. Sun, *Energy Environ. Sci.*, 2014, **7**, 329-334; (b) W. T. Eckenhoff, W. R. McNamara, P. Du and R. Eisenberg, *Biochim. Biophys. Acta*, 2013, **1827**, 958-973; (c) M. Guttentag, A. Rodenberg, C. Bachmann, A. Senn, P. Hamm and R. Alberto, *Dalton Trans.*, 2013, **42**, 334-337; (d) C. C. L. McCrory, C. Uyeda and J. C. Peters, *J. Am. Chem. Soc.*, 2012, **134**, 3164-

3170; (e) V. Artero, M. Chavarot-Kerlidou and M. Fontecave, *Angew. Chem. Int. Ed.*, 2011, **50**, 7238-7266; (f) Y. Sun, J. P. Bigi, N. A. Piro, M. L. Tang, J. R. Long and C. J. Chang, *J. Am. Chem. Soc.*, 2011, **133**, 9212-9215; (g) J. P. Bigi, T. E. Hanna, W. H. Harman, A. Chang and C. J. Chang, *Chem. Comm.*, 2010, **46**, 958-960; (h) P. Du, J. Schneider, G. Luo, W. W. Brennessel and R. Eisenberg, *Inorg. Chem.*, 2009, **48**, 4952-4962; (i) P.-A. Jacques, V. Artero, J. Pécaut and M. Fontecave, *Proc. Natl. Acad. Sci.*, 2009, **106**, 20627-20632; (j) X. Hu, B. S. Brunschwig and J. C. Peters, *J. Am. Chem. Soc.*, 2007, **129**, 8988-8998; (k) P. Connolly and J. H. Espenson, *Inorg. Chem.*, 1986, **25**, 2684-2688; (l) B. J. Fisher and R. Eisenberg, *J. Am. Chem. Soc.*, 1980, **102**, 7361-7363.

4 (a) P. Zhang, M. Wang, Y. Yang, D. Zheng, K. Han and L. Sun, *Chem. Comm.*, 2014, **50**, 14153-14156; (b) Z. Han, L. Shen, W. W. Brennessel, P. L. Holland and R. Eisenberg, *J. Am. Chem. Soc.*, 2013, **135**, 14659-14669; (c) O. R. Luca, S. J. Konezny, J. D. Blakemore, D. M. Colosi, S. Saha, G. W. Brudvig, V. S. Batista and R. H. Crabtree, *New J. Chem.*, 2012, **36**, 1149-1152; (d) U. J. Kilgore, J. A. S. Roberts, D. H. Pool, A. M. Appel, M. P. Stewart, M. Rakowski DuBois, W. G. Dougherty, W. S. Kassel, R. M. Bullock and D. L. DuBois, *J. Am. Chem. Soc.*, 2011, **133**, 5861-5872; (e) A. D. Wilson, R. H. Newell, M. J. McNevin, J. T. Muckerman, M. Rakowski DuBois and D. L. DuBois, *J. Am. Chem. Soc.*, 2006, **128**, 358-366; (f) J.-P. Collin, A. Jouaiti and J.-P. Sauvage, *Inorg. Chem.*, 1988, **27**, 1986-1990.

5 (a) D. V. Esposito and J. G. Chen, *Energy Environ. Sci.*, 2011, **4**, 3900-3912; (b) R. B. Gordon, M. Bertram and T. E. Graedel, *Proc. Natl. Acad. Sci.*, 2006, **103**, 1209-1214; (c) M. Kirch, J.-M. Lehn and J.-P. Sauvage, *Helv. Chim. Acta*, 1979, **62**, 1345-1384.

6 (a) T. Sakai, D. Mersch and E. Reisner, *Angew. Chem. Int. Ed.*, 2013, **52**, 12313-12316; (b) P. D. Tran and J. Barber, *Phys. Chem. Chem. Phys.*, 2012, **14**, 13772-13784; (c) H. Krassen, A. Schwarze, B. Friedrich, K. Ataka, O. Lenz and J. Heberle, *ACS Nano*, 2009, **3**, 4055-4061; (d) E. Reisner, D. J. Powell, C. Cavazza, J. C. Fontecilla-Camps and F. A. Armstrong, *J. Am. Chem. Soc.*, 2009, **131**, 18457-18466; (e) K. A. Vincent, A. Parkin and F. A. Armstrong, *Chem. Rev.*, 2007, **107**, 4366-4413.

7 (a) Y. Gao, X. Ding, J. Liu, L. Wang, Z. Lu, L. Li and L. Sun, *J. Am. Chem. Soc.*, 2013, **135**, 4219-4222; (b) A. Krawicz, J. Yang, E. Anzenberg, J. Yano, I. D. Sharp and G. F. Moore, *J. Am. Chem. Soc.*, 2013, **135**, 11861-11868; (c) G. F. Moore and I. D. Sharp, *J. Phys. Chem. Lett.*, 2013, **4**, 568-572; (d) L. Alibabaei, M. K. Brennaman, M. R. Norris, B. Kalanyan, W. Song, M. D. Losego, J. J. Concepcion, R. A. Binstead, G. N. Parsons and T. J. Meyer, *Proc. Natl. Acad. Sci.*, 2013, **110**, 20008-20013.

8 (a) M. Wang, L. Chen, X. Li and L. Sun, *Dalton Trans.*, 2011, **40**, 12793-12800; (b) C. J. Curtis, A. Miedaner, R. Ciancanelli, W. W. Ellis, B. C. Noll, M. Rakowski DuBois and D. L. DuBois, *Inorg. Chem.*, 2003, **42**, 216-227.

9 M. A. Gross, A. Reynal, J. R. Durrant and E. Reisner, *J. Am. Chem. Soc.*, 2014, **136**, 356-366.

10 A. Dutta, S. Lense, J. Hou, M. H. Engelhard, J. A. S. Roberts and W. J. Shaw, *J. Am. Chem. Soc.*, 2013, **135**, 18490-18496.

11 (a) A. K. Das, M. H. Engelhard, R. M. Bullock and J. A. S. Roberts, *Inorg. Chem.*, 2014, **53**, 6875-6885; (b) A. Le Goff, V. Artero, B. Jousselme, P. D. Tran, N. Guillet, R. Métayé, A. Fihri, S. Palacin and M. Fontecave, *Science*, 2009, **326**, 1384-1387.

12 C. A. Caputo, M. A. Gross, V. W. Lau, C. Cavazza, B. V. Lotsch and E. Reisner, *Angew. Chem. Int. Ed.*, 2014, **53**, 11538-11542.

13 F. Wang, W.-G. Wang, X.-J. Wang, H.-Y. Wang, C.-H. Tung and L.-Z. Wu, *Angew. Chem. Int. Ed.*, 2011, **50**, 3193-3197.

14 S. Pullen, H. Fei, A. Orthaber, S. M. Cohen and S. Ott, *J. Am. Chem. Soc.*, 2013, **135**, 16997-17003.

15 F. Quentel, G. Passard and F. Gloaguen, *Energy Environ. Sci.*, 2012, **5**, 7757-7761.

16 (a) D. W. Wakerley and E. Reisner, *Phys. Chem. Chem. Phys.*, 2014, **16**, 5739-5746; (b) M. Razavet, V. Artero and M. Fontecave, *Inorg. Chem.*, 2005, **44**, 4786-4795.

17 (a) B. H. Solis, Y. Yu and S. Hammes-Schiffer, *Inorg. Chem.*, 2013, **52**, 6994-6999; (b) B. H. Solis and S. Hammes-Schiffer, *Inorg. Chem.*, 2011, **50**, 11252-11262; (c) J. T. Muckerman and E. Fujita, *Chem. Comm.*, 2011, **47**, 12456-12458; (d) B. H. Solis and S. Hammes-Schiffer, *J. Am. Chem. Soc.*, 2011, **133**, 19036-19039; (e) T. Lazarides, T. McCormick, P. Du, G. Luo, B. Lindley and R. Eisenberg, *J. Am. Chem. Soc.*, 2009, **131**, 9192-9194; (f) J. L. Dempsey, B. S. Brunschwig, J. R. Winkler and H. B. Gray, *Acc. Chem. Res.*, 2009, **42**, 1995-2004; (g) P. Du, K. Knowles and R. Eisenberg, *J. Am. Chem. Soc.*, 2008, **130**, 12576-12577; (h) C. Baffert, V. Artero and M. Fontecave, *Inorg. Chem.*, 2007, **46**, 1817-1824; (i) X. Hu, B. M. Cossairt, B. S. Brunschwig, N. S. Lewis and J. C. Peters, *Chem. Comm.*, 2005, DOI: 10.1039/B509188H, 4723-4725.

18 F. Lakadamyali, M. Kato, N. M. Muresan and E. Reisner, *Angew. Chem. Int. Ed.*, 2012, **51**, 9381-9384.

19 (a) B. S. Veldkamp, W.-S. Han, S. M. Dyar, S. W. Eaton, M. A. Ratner and M. R. Wasielewski, *Energy Environ. Sci.*, 2013, **6**, 1917-1928; (b) A. Fihri, V. Artero, A. Pereira and M. Fontecave, *Dalton Trans.*, 2008, DOI: 10.1039/B812605B, 5567-5569; (c) A. Fihri, V. Artero, M. Razavet, C. Baffert, W. Leibl and M. Fontecave, *Angew. Chem. Int. Ed.*, 2008, **47**, 564-567.

20 (a) F. Lakadamyali, M. Kato and E. Reisner, *Farad. Discuss.*, 2012, **155**, 191-205; (b) F. Lakadamyali and E. Reisner, *Chem. Comm.*, 2011, **47**, 1695-1697.

21 X.-W. Song, H.-M. Wen, C.-B. Ma, H.-H. Cui, H. Chen and C.-N. Chen, *RSC Adv.*, 2014, **4**, 18853-18861.

22 (a) A. Krawicz, D. Cedeno and G. F. Moore, *Phys. Chem. Chem. Phys.*, 2014, **16**, 15818-15824; (b) Z. Ji, M. He, Z. Huang, U. Ozkan and Y. Wu, *J. Am. Chem. Soc.*, 2013, **135**, 11696-11699.

23 T. M. McCormick, Z. Han, D. J. Weinberg, W. W. Brennessel, P. L. Holland and R. Eisenberg, *Inorg. Chem.*, 2011, **50**, 10660-10666.

24 N. M. Muresan, J. Willkomm, D. Mersch, Y. Vaynzof and E. Reisner, *Angew. Chem. Int. Ed.*, 2012, **51**, 12749-12753.

25 (a) A. Bhattacharjee, E. S. Andreiadis, M. Chavarot-Kerlidou, M. Fontecave, M. J. Field and V. Artero, *Chem. Eur. J.*, 2013, **19**, 15166-15174; (b) P. Zhang, P.-A. Jacques, M. Chavarot-Kerlidou, M. Wang, L. Sun, M. Fontecave and V. Artero, *Inorg. Chem.*, 2012, **51**, 2115-2120; (c) B. Probst, M. Guttentag, A. Rodenberg, P. Hamm and R. Alberto, *Inorg. Chem.*, 2011, **50**, 3404-3412.

26 E. S. Andreiadis, P.-A. Jacques, P. D. Tran, A. Leyris, M. Chavarot-Kerlidou, B. Jousselme, M. Matheron, J. Pécaut, S. Palacin, M. Fontecave and V. Artero, *Nat. Chem.*, 2013, **5**, 48-53.

27 M. R. J. Scherer, N. M. Muresan, U. Steiner and E. Reisner, *Chem. Comm.*, 2013, **49**, 10453-10455.

28 F. Tayyari, D. E. Wood, P. E. Fanwick and R. E. Sammelson, *Synthesis*, 2008, DOI: DOI 10.1055/s-2007-990945, 279-285.

29 L. G. Marzilli, A. Gerli and A. M. Calafat, *Inorg. Chem.*, 1992, **31**, 4617-4627.

30 J. Xie, Q. Zhou, C. Li, W. Wang, Y. Hou, B. Zhang and X. Wang, *Chem. Comm.*, 2014, **50**, 6520-6522.

31 V. Fourmond, S. Canaguier, B. Golly, M. J. Field, M. Fontecave and V. Artero, *Energy Environ. Sci.*, 2011, **4**, 2417-2427.

32 J. L. Dempsey, J. R. Winkler and H. B. Gray, *J. Am. Chem. Soc.*, 2010, **132**, 1060-1065.

33 J. J. Spivey and K. M. Dooley, *Catalysis*, The Royal Society of Chemistry, Cambridge, 2007.

34 A. Adin and J. H. Espenson, *Inorg. Chem.*, 1972, **11**, 686-688.

35 (a) E. Reisner, V. B. Arion, M. F. C. Guedes da Silva, R. Lichtenecker, A. Eichinger, B. K. Keppler, V. Y. Kukushkin and A. J. L. Pombeiro, *Inorg. Chem.*, 2004, **43**, 7083-7093; (b) A. B. P. Lever, *Inorg. Chem.*, 1990, **29**, 1271-1285.

36 P. G. Hoertz, Z. Chen, C. A. Kent and T. J. Meyer, *Inorg. Chem.*, 2010, **49**, 8179-8181.

37 H. Park, E. Bae, J.-J. Lee, J. Park and W. Choi, *J. Phys. Chem. B*, 2006, **110**, 8740-8749.

38 V. Balzani, G. Bergamini, F. Marchioni and P. Ceroni, *Coord. Chem. Rev.*, 2006, **250**, 1254-1266.

39 F. Lakadamyali, A. Reynal, M. Kato, J. R. Durrant and E. Reisner, *Chem. Eur. J.*, 2012, **18**, 15464-15475.

40 (a) Y. Xu and M. A. A. Schoonen, *Am. Mineral.*, 2000, **85**, 543-556; (b) J. M. Bolts and M. S. Wrighton, *J. Phys. Chem.*, 1976, **80**, 2641-2645.

41 K. Sayama and H. Arakawa, *J. Phys. Chem.*, 1993, **97**, 531-533.

42 A. Reynal, J. Willkomm, N. M. Muresan, F. Lakadamyali, M. Planells, E. Reisner and J. R. Durrant, *Chem. Comm.*, 2014, **50**, 12768-12771.

43 (a) H. Sun and M. Z. Hoffman, *J. Phys. Chem.*, 1994, **98**, 11719-11726; (b) K. Kalyanasundaram, J. Kiwi and M. Grätzel, *Helv. Chim. Acta*, 1978, **61**, 2720-2730.

44 L. I. Simándi, Z. Szeverényi and É. Budó-Záhonyi, *Inorg. Nucl. Chem. Lett.*, 1975, **11**, 773-777.

45 E. B. Hulley, P. T. Wolczanski and E. B. Lobkovsky, *J. Am. Chem. Soc.*, 2011, **133**, 18058-18061.

46 S. Cobo, J. Heidkamp, P.-A. Jacques, J. Fize, V. Fourmond, L. Guetaz, B. Jousselme, V. Ivanova, H. Dau, S. Palacin, M. Fontecave and V. Artero, *Nat Mater*, 2012, **11**, 802-807.

47 J. Dong, M. Wang, X. Li, L. Chen, Y. He and L. Sun, *ChemSusChem*, 2012, **5**, 2133-2138.

48 A. Reynal, F. Lakadamyali, M. A. Gross, E. Reisner and J. R. Durrant, *Energy Environ. Sci.*, 2013, **6**, 3291-3300.

49 S. Varma, C. E. Castillo, T. Stoll, J. Fortage, A. G. Blackman, F. Molton, A. Deronzier and M.-N. Collomb, *Phys. Chem. Chem. Phys.*, 2013, **15**, 17544-17552.

Table of Contents Artwork
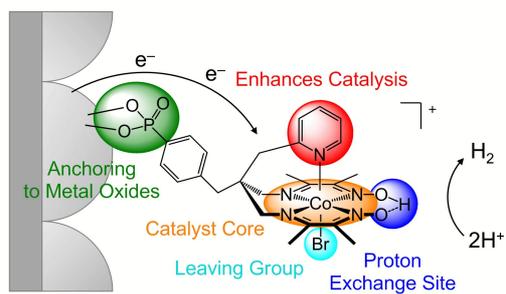
Rational ligand design was employed to improve the proton reduction activity of an immobilised cobalt diimine-dioxime catalyst.